Int J Biometeorol (2017) 61:2059–2071
DOI 10.1007/s00484-017-1403-4

ORIGINAL PAPER

On the ratio of intercellular to ambient CO_2 (c_i/c_a) derived from ecosystem flux

Zheng-Hong Tan[1] · Zhi-Xiang Wu[2] · Alice C. Hughes[3] · Douglas Schaefer[4] · Jiye Zeng[5] · Guo-Yu Lan[2] · Chuang Yang[2] · Zhong-Liang Tao[2] · Bang-Qian Chen[2] · Yao-Hua Tian[6] · Liang Song[4] · Muhammad Tahir Jatoi[1,2] · Jun-Fu Zhao[1] · Lian-Yan Yang[1]

Received: 28 January 2016 / Revised: 13 June 2017 / Accepted: 29 June 2017 / Published online: 13 July 2017

Abstract The ratio of intercellular to ambient CO_2 concentrations (c_i/c_a) plays a key role in ecophysiology, micrometeorology, and global climatic change. However, systematic investigation on c_i/c_a variation and its determinants are rare. Here, the c_i/c_a was derived from measuring ecosystem fluxes in an even-aged monoculture of rubber trees (*Hevea brasiliensis*). We tested whether c_i/c_a is constant across environmental gradients and if not, which dominant factors control c_i/c_a variations. Evidence indicates that c_i/c_a is not a constant. The c_i/c_a exhibits a clear "*V*"-shaped diurnal pattern and varies across the environmental gradient. Water vapor pressure deficit (*D*) is the dominant factor controls over the c_i/c_a variations. c_i/c_a consistently decreases with increasing *D*. c_i/c_a decreases with square root of *D* as predicted by the optimal stomatal model. The *D*-driving single-variable model could simulate c_i/c_a as well as that of sophisticated model. Many variables function on longer timescales than a daily cycle, such as soil water content, could improve c_i/c_a model prediction ability. Ecosystem flux can be effectively used to calculate c_i/c_a and use it to better understand various natural cycles.

Keywords Canopy conductance · Photosynthesis · Eddy covariance · Water vapor deficit · Ecosystem model

✉ Zhi-Xiang Wu
wzxrri@163.com

[1] Ecology Program, Institute for Tropical Agriculture and Forestry, Hainan University, Haikou 570228, China

[2] Rubber Research Institute, Chinese Academy of Tropical Agricultural Sciences, Danzhou 571737, China

[3] Centre for Integrative Conservation, Xishuangbanna Tropical Botanical Garden, Chinese Academy of Sciences, Menglun 666303, China

[4] Key Lab of Tropical Forest Ecology, Xishuangbanna Tropical Botanical Garden, Chinese Academy of Sciences, Kunming 666303, China

[5] National Institute for Environmental Studies, Tsukuba 305-0053, Japan

[6] Yunnan Institute of Tropical Crops, Jinghong 666100, China

Introduction

In April 2014, the global mean atmospheric CO_2 concentration exceeded 400 ppm for the first time (http://www.esrl.noaa.gov/gmd/ccgg/trends/). CO_2 is both a greenhouse gas responsible for warming the earth and the substrate for leaf photosynthesis. Increasing CO_2 concentrations will not only warm the earth surface but also benefit photosynthesis and enhance water use efficiency of C_3 plants (Keenan et al. 2013). CO_2's complicated role makes it a central concern for global climate change studies.

Photosynthesis studies have demonstrated that plants do not directly sense ambient CO_2 in the air (c_a) but rather use intercellular CO_2 (c_i) (Landsberg and Sands 2011). A well-resolved c_i is thus important for photosynthetic research, including photosynthesis models (Collatz et al. 1991). Studies of stomatal behavior provide useful information of c_i under a variety of conditions. In a laboratory experiment, Wong et al. (1979) found that stomatal conductance (g_s) changes proportionally with photosynthesis rate (*A*), which implies that c_i will remain constant when c_a is kept constant. This concept has been adopted in modeling studies, i.e., Norman (1982) approximate $c_i = 0.80\ c_a$ for C_3 plants. Many stomatal models have utilized the first model produced (36 years ago; Wong et al. 1979), built upon a range of conditions and scenarios (Damour et al. 2010). These stomatal models give different c_i

predictions, and a consistent c_i solution cannot be developed until consensus is reached on an accurate stomatal model.

Systematic investigations of c_i or c_i/c_a behavior and its response to environmental variables have rarely been conducted. Most studies of c_i/c_a have not examined general responses but have had a narrower focus, such as responses to drought (Brodribb 1996) and water vapor deficit (Mortazavi et al. 2005), or scaling up c_i/c_a to the canopy (Tissue et al. 2006). Moreover, most studies have used leaf chamber measurements collected under sunny conditions or isotope recordings that cover only a narrow range of c_i/c_a values, while a wider range of environmentally relevant conditions have not been reported.

Here, we present a systematic study on c_i/c_a which incorporates ecosystem flux measurements, and dynamic patterns of c_i/c_a behavior. We would like to address three specific questions in the study: (i) whether c_i/c_a is a constant; (ii) if not, how does it vary over time and how is it influenced by various environmental factors; and (iii) can an accurate model be developed to simulate c_i/c_a variation.

Materials and methods

Theory

Based on Fick's first law of diffusion (Fick 1855), carbon and water vapor fluxes through stomata can be expressed as follows:

$$A = g_{sc}(c_a - c_i) \quad \text{and} \tag{1}$$

$$E = g_{sv}(w_i - w_a), \tag{2}$$

where A is the photosynthetic assimilation rate, g is the stomatal conductance, g_{sc} is the stomatal conductance for CO_2, g_{sv} is the stomatal conductance for water vapor, c_a is the ambient CO_2 concentration, c_i is the intercellular CO_2 concentration, E is the transpiration rate, w_i is the intercellular water vapor concentration, and w_a is the ambient water vapor concentration.

Rearranging Eq. (1), we present c_i as

$$c_i = c_a - \frac{A}{g_{sc}}. \tag{3}$$

c_a and A can be measured with gas exchange chambers and infrared gas analyzers, but two variables remain unknown in Eq. (3): c_i and g_{sc}. An additional equation can solve c_i. The relative diffusivity of water vapor to CO_2 is a fixed value of around 1.6 (Farquhar and Sharkey 1982). Incorporating Eq. (2) into Eq. (3), we obtain

$$c_i = c_a - \frac{1.6A(w_i - w_a)}{E}. \tag{4}$$

Water vapor concentration can be expressed as a unit of pressure to obtain

$$c_i = c_a - \frac{1.6A}{E}\frac{(e_i - e_a)}{P_a}, \tag{5}$$

where e_i is the intercellular water vapor pressure, e_a is the ambient water vapor pressure, and P_a is the air pressure, c_i and c_a in the unit of ppm. Equation (5) explicitly enables the calculation of c_i from gas fluxes along with measurements of environmental parameters.

The "big leaf" concept

Theories and empirical models of c_i/c_a have previously been predominantly based on leaf measurements. A frequently used concept in canopy studies regards the canopy from a leaf level as a single big leaf (Norman 1982). We can slightly modify Eq. (5) to calculate the bulk intercellular CO_2 in the canopy (denoted as c_i, the same as at the leaf level) by taking the big leaf concept as

$$c_i = c_a - \frac{1.6A_c}{LE_{dry}/\Lambda}\frac{(e_s(T_c) - e_a)}{P_a}, \tag{6}$$

where A_c is the gross canopy photosynthesis assimilation rate (μmol m^{-2} s^{-1}), LE_{dry} is the latent heat flux from dry closed canopy (LE) (W m^{-2}), Λ is the latent heat of vaporization of water (J mol^{-1}), e_s is the saturated water vapor pressure at a specific temperature (Pa), and T_c is the canopy temperature (°C).

Bulk canopy conductance (g_c) is important for addressing and understanding c_i/c_a behavior (see Eq. (1) replacing g_{sc} as g_c). Here, it is calculated by inverting the Penman–Monteith equation as follows:

$$\frac{1}{g_c} = \frac{\rho C_p D}{\gamma LE} + \frac{\frac{H}{LE}\frac{\Delta}{\gamma} - 1}{g_a}, \tag{7}$$

where ρ is the air density (kg m^{-3}), C_p is the specific heat of air at constant pressure (J kg^{-1} K^{-1}), γ is the psychrometric constant (kPa K^{-1}), D is the water vapor deficit (kPa), H is the sensible heat flux (W m^{-2}), and Δ is the rate of change of saturated water pressure with temperature (kPa K^{-1}). g_a is the aerodynamic conductance, which is calculated as

$$\frac{1}{g_a} = \frac{u}{u_*^2} + \frac{B^{-1}}{u_*}, \tag{8}$$

where u is the mean wind speed (m s^{-1}), u_* is the friction velocity (m s^{-1}), and B^{-1} is the dimensionless sub-layer Stanton number (Blanken et al. 1997).

Predictions of c_i/c_a behavior in empirical models

Empirical models have been proposed to describe c_i/c_a behavior. These models can be categorized into four classes.

(1) **c_i/c_a is constant and independent of environmental variables.** It has been suggested that c_i/c_a remains constant via stomatal regulation (personal communications, J. A. Berry, in Farquhar and Wong (1984)). Wong et al. (1979) tested this hypothesis experimentally and obtained a linear relationship between A and g_{sc} under different light intensities. The slope of the A–g_{sc} regression line varies among species but not within species.

(2) **c_i/c_a is dependent on light intensity**. The dependence of c_i/c_a on light intensity (Q) was found experimentally in a study of photosynthetic response to irradiance (Ball and Critchley 1982), and empirically modeled for stomatal conductance (Farquhar and Wong 1984). Low light intensity limits g_{sc}, and c_i/c_a decreases rapidly in the light-limiting period as light intensity increases (Farquhar and Wong 1984). Outside the light-limiting period, c_i/c_a remained constant. This relationship can be expressed as

$$\frac{c_i}{c_a} = \begin{cases} \propto Q & if \;\; Q < Q_c \\ cons & if \;\; Q \geq Q_c \end{cases}, \tag{9}$$

where Q_c is the critical Q when c_i/c_a shifts from light dependence to a constant value.

(3) **c_i/c_a is dependent on water vapor pressure deficit**. Stomatal conductance strongly depends on a deficit of water vapor pressure (D) (Zhang and Nobel 1996). Inferred or derived from these stomatal behavior models, several models relate c_i/c_a to D. The optimal stomatal behavior theory predicts a linear relationship between c_i/c_a and D (Cowan and Farquhar 1977), and one combined model of stomatal behavior and isotope analysis suggests that c_i/c_a is linearly correlated to the square root of D (Lloyd and Farquhar 1994). The c_i/c_a was also found to exponentially decay with time-lagged D (Mortazavi et al. 2005).

(4) **c_i/c_a is dependent on stomatal conductance**. Katul et al. (2000) proposed a hybrid model that relates c_i/c_a to g_{sc}. The model expresses c_i/c_a as

$$\frac{c_i}{c_a} = \begin{cases} \dfrac{g_{sc} + b\Big/c_a}{a + g_{sc}} & if \; g_{sc} < g_{critical} \\ R_c = \dfrac{g_{critical} + b\Big/c_a}{a + g_{critical}} & if \; g_{sc} \geq g_{critical} \end{cases}, \tag{10}$$

where R_c is c_i/c_a under nearly constant level; a and b are the parameters derived from the A–c_i curve, which was determined by nonlinear regression in this study; and $g_{critical}$ is the critical value for g_{sc}.

Experimental site

To minimize variability induced by species diversity, we selected a monospecific tropical rubber plantation for this study. Rubber tree, with its scientific name as *Hevea brasiliensis*, is native to Brazil and the Guianas, but most of the world's rubber trees was planted in southeast Asia. Rubber tree is a deciduous tree usually 15–25 m tall in cultivation. It can grow to 40 m tall and live for 100 years in the wild. Plantation trees, however, are rarely exceed 25 m and were cut down about 25–35 years after planted. The *H. brasiliensis* seedlings were planted in 2001 with a density of 476 individuals per hectare, and rubbing tapping started in 2009. Mean canopy height is 13.0 m and mean diameter at breast height is 22.77 cm (data from 2013).

The geographic location of the site (109° 28′ 30″ E, 19° 32′ 47″ N) is in Danzhou, Hainan, China. Mean elevation there is 144 m. The climate is dominated by tropical monsoon regime; there are clear dry (November to April next year) and wet seasons (May through October). Mean annual temperature is 23.5 °C. Annual rainfall varied strongly among years (1607~2000 mm), but more than 70% of the rainfall occurred in July, August, and September. Solar radiation is about 486 kJ cm^{-2} with 2100 sunshine hours. Mean relative humidity is 83% and mean wind speed is 2~2.5 m s^{-1} (Wu et al. 2015). The terrain presents slopes less than 5°.

Instrumentation and observation

A 50-m micrometeorological tower was established to monitoring fluxes between rubber plantation and atmosphere. Major instruments on the tower can be categorized into two parts: the eddy flux system and routine microclimatic system. The eddy flux system consists of a sonic anemometer (CSAT-3, Campbell Scientific Inc., Logan, UT, USA) which measures three-dimensional wind velocity, and an open-path infrared gas analyzer (Li-7500, Li-Cor Inc., USA) was amount at the height of 25 m. Eddy flux data was sampled at the frequency of 10 Hz controlled by a data logger (model CR3000, Campbell Scientific Inc., USA). The microclimatic system includes rain gauge (TE525MM, Texas Electronics, USA) at 50-m height, temperature and humidity sensor (model HMP45C sensor, Vaisala, Finland) at 33-m height, wind cup (Met 010C-1, Met One Instrument, USA) at 33-m height, photosynthetic active radiation quantum sensor (LQS70–10, Apogee Instruments, Logan, UT, USA) at 30-m height, infrared thermometer (IRTS-P, Apogee Instruments, Logan, UT,

USA) at 30-m height, time-domain reflectometry soil water content sensor (TDR; model CS616, Campbell Scientific Inc.) at 5-cm depth, net radiation radiometer (CRN-1, Kipp Zonen, the Netherlands) at 25-m height, soil temperature sensor (TCAV-L, Campbell, USA) at 5-cm depth, and soil heat flux (HFP01, Hukseflux, the Netherlands) at 5-cm depth. Microclimatic data was retrieved each 10 s, and the 30-min averages or sums are recorded by a data logger CR3000.

Flux calculation

Eddy fluxes were calculated as the covariance between vertical wind speed components and the respective scalars,

$$F_x = \overline{w'x'}, \tag{11}$$

where F_x is the eddy flux of x scalars (i.e., CO_2, water vapor, and temperature), w is the vertical wind speed, the overbar indicates averaging, primes indicate the perturbations to mean values, and the averaging period was 30 min.

Sensible (H_s) and latent heat fluxes (LE) were directly calculated from the covariance calculated in Eq. (11). Heat flux storage changes were excluded from the analysis, being less than 5% in total. We did not perform energy balance closure corrections on H_s or LE. Net ecosystem exchange (NEE) was calculated as the sum of eddy carbon flux (F_c) and storage flux (F_s) as follows:

$$NEE = F_c + F_s = F_c + \frac{dc}{dt} z_r, \tag{12}$$

where dc/dt is the change of CO_2 concentration with time and z_r is the measurement height (Wu et al. 2013). Data collected from a CO_2 profile system (eight levels 1.5, 6, 10, 15, 25, 33, 41, 50 m) was used to calculate F_s. The profile system used an infrared gas analyzer (model Li-840, Li-Cor, USA) to measure CO_2 concentration.

In the processes of calculating F_c, several common steps were included.

(i) *Axis rotation*. Rotating the coordinate to make mean vertical wind speed is equal to zero. The double-rotation method was used to make zero mean vertical wind speed in this study (Tanner and Thurtell 1969).

(ii) *WPL correction*. The changes of air density (i.e., caused by temperature thermal expansion) could affect the measured fluctuations in CO_2, H_2O, and other gases. We used the WPL correction to correct for changes in air density as proposed by Webb et al. (1980).

(iii) *Frequency loss correction*. Some high or low flux signals may be lost due to sensor performance; to compensate for these losses, we apply frequency loss correction as recommended by Burba and Anderson (2010).

The canopy photosynthesis assimilation rate (A_c) was calculated as follows:

$$A_c = -\left(NEE_{\text{day}} - R_{\text{day}}\right), \tag{13}$$

where NEE_{day} is the daytime NEE and R_{day} is the daytime respiration; the "minus" is due to a discipline convention. R_{day} was estimated from nighttime respiration (R_{night}) and temperature. There was no photosynthesis at night. Nighttime NEE thus equals R_{night}. After screening low turbulence, rainfall, and theoretically unreasonable and noisy data, R_{night} was related to temperature. R_{day} was estimated by using the regression equation and measured under daytime temperatures.

Eddy covariance-based evapotranspiration (LE/Λ) is the sum of transpiration and evaporation. The evaporation component predominantly comes from wet canopy evaporation and forest floor surface evaporation. The contribution of forest floor surface evaporation is usually very small in forests with a fully closed dense canopy (Kelliher et al. 1995; Keenan et al. 2013). Thus, we only selected data when trees had a fully closed canopy and removed data during leaf shedding and flushing. To avoid erroneous data from a wet canopy, we excluded data during rainfall. After removing these data, the remaining data for a dry and fully closed canopy LE (LE_{dry}) was used to estimate transpiration.

Most previous studies at the leaf level were conducted under light-saturated photosynthesis. To make our results comparable to those at leaf levels, light-saturated data were selected for further response analysis. We fitted a rectangular photosynthesis light response curve (Eq. (14)) to our observations,

$$-NEE = \alpha P_{\max} P_{FD} \Big/ (\alpha P_{FD} + P_{\max}) - R_d, \tag{14}$$

where α is the apparent quantum yield, $P_{\max}$ is the light-saturated photosynthesis rate, P_{FD} is the photosynthetic active radiation flux density, and R_d is the ecosystem respiration at zero light. The light saturation point was determined as $P_{\max}/\alpha$.

Flux data quality assessment and control

As a discipline convention, it is necessary to report the quality assessment and control (QA/QC) information on eddy flux data processing. We did the following QA/QC on our eddy flux data (Wu 2013):

(i) *Steady state test (SST) and integrated turbulence characteristic test (ITC)*. The SST and ITC were carried to assess the data quality. Data were categorized into different quality levels after SST and ITC. All SST and ITC were implemented according to Foken and Wichura (1996).

(ii) *Energy balance closure analysis*. The overall energy balance closure ratio for the whole year 2010 with 30-min resolution data is 0.8676.

(iii) *Flux source area analysis*. We used the method provided by Schimid (1994) to estimate source area of eddy flux. The source area "fetch" is 100~785 m in prevailing wind direction and −251~251 m in the cross wind direction (Wu et al. 2012). Vegetation in source areas is also predominantly rubber trees.

(iv) *Spike detection and exclusion*. Spikes may be generated by electronic noises or some other physical reasons. We adopted Vickers and Mahrt (1997)'s method to detect and remove these spikes. All signals that are more than six times the standard deviation for a given averaging period are treated as outliers and removed.

(v) *u* filtering*. Nighttime flux was frequently underestimated due to weak turbulence, and *u** filtering (*u** is the friction velocity) was used to minimize this potential underestimation. The threshold *u** used in our case is a fixed value of 0.12 m s^{-1}. All values below the *u** threshold were removed.

(vi) *Data period selection*. The eddy flux tower started measurement in November 2009; however, in July 2011, typhoon Nasha destroyed some instruments, which were repaired the following year. Consequently, we selected the whole year data between January 1 and December 31, 2010 for this study.

Modeling the c_i/c_a

We would like to ask whether these models described in the "Predictions of c_i/c_a behavior in empirical models" section could be used to simulate c_i/c_a, and determine which model has the strongest prediction ability. We tested three major models in the study (Jarvis, Medlyn, and Katul models). Both Medlyn and Katul models could be categorized into optimization theory which originally suggested by Cowan and Farquhar (1977).

(i) The Jarvis model is for predicting g_c, not for c_i/c_a. It is expressed as

$$g_c = f_1(P_{FD}) f_2(D) f_3(S_w) f_4(c_a) \ldots f_n(x), \tag{15}$$

where subscript 1 to *n* represents the function number and *x* is the input model driver. It has been shown above that c_i/c_a could well related to g_c as (Katul et al. 2000)

$$c_i \Big/ c_a = {}^{a}\frac{g_c + b \Big/ c_a}{a + g_c}. \tag{16}$$

We therefore incorporate Eq. (15) into Eq. (16) to enable the multifactor driving Jarvis model that could be used for predicting c_i/c_a. In practical use, there are different functions and combinations for Jarvis-type stomatal models. Here, we used six expressions. They are

$$\textit{Expression}\ 1 : g_c = f_1(P_{FD}) f_2(D) = \frac{P_{FD}(1-dD)}{(c + P_{FD})}, \tag{17}$$

$$\textit{Expression}\ 2 : g_c = f_1(P_{FD}) f_2(D) = \frac{P_{FD}\left(1-d\sqrt{D}\right)}{(c + P_{FD})}, \tag{18}$$

$$\textit{Expression}\ 3 : g_c = f_1(P_{FD}) f_2(D) = \frac{P_{FD}}{(c + P_{FD})(d + D)}, \tag{19}$$

$$\textit{Expression}\ 4 : g_c = f_1(P_{FD}) f_2(D) = \frac{1-\exp(cP_{FD})}{(d + D)}, \tag{20}$$

$$\textit{Expression}\ 5 : g_c = f_1(P_{FD}) f_2(D) f_3(S_w) = \frac{P_{FD}\exp(mS_w)}{(c + P_{FD})(d + D)}, \tag{21}$$

$$\textit{Expression}\ 6 : g_c = f_1(P_{FD}) f_2(D) f_3(S_w) f_4(T_a) = \frac{P_{FD}\exp(mS_w)\exp(jT_a)}{(c + P_{FD})(d + D)}, \tag{22}$$

where *c*, *d*, *m*, and *j* are the fitting parameters. *D* is the water vapor deficit, S_w is the soil water content (here specified to 5-cm depth), and T_a is the air temperature (here specified to air temperature most near the canopy).

(ii) The Medlyn model is a stomatal optimization model which assumes that optimization occurred during light-limited condition (Medlyn et al. 2011). The mathematic expression is very simple as

$$\frac{c_i}{c_a} = \frac{g_1}{g_1 + \sqrt{D}}, \tag{23}$$

where g_1 is a parameter which varied among but not within a specific species.

(iii) The Katul model is also founded its basis on stomatal optimization theory (Katul et al. 2010). Katul model describes stomatal optimization under light-saturated condition,

$$\frac{c_i}{c_a} = 1 - \sqrt{\frac{1.6\lambda D}{c_a}}, \tag{24}$$

where λ is the marginal water use efficiency which is a fitted parameter in the study.

Statistical analysis

All statistical analyses were performed by using the MATLAB 7.0 (MathWorks, USA). Linear regression and nonlinear regression were accomplished with the polyfit and nlinfit command, respectively.

Results

A–g curve (A_c–g_c curve at canopy scale)

The *A–g* curve is the basis for our study into c_i/c_a behavior, as shown in Eq. (3). Figure 1 shows the canopy-scale *A–g* curve (A_c–g_c curve). A_c increases with g_c for over 80% of the data (g_c < 1.5 cm s^{-1}) with a positive quasi-linear correlation. We say quasi-linear and not linear because a quadratic function (dashed line in Fig. 1; Pearson's $r = 0.6609$) could give a better statistically fit than linear one (solid line in Fig. 1; $r = 0.6541$). A_c–g_c relationship becomes very sparse under high g_c levels (>1.5 cm s^{-1}). These sparse points mostly are early morning data when g_c is near its peak but light is limited.

The temporal dynamics of c_i/c_a

The time series of c_i/c_a was shown in Fig. 2. Most of the values varied within 0.5 and 1. The block averaging for all points was 0.7448. A few of these points have the value larger than the theoretical maximum 1.0. The seasonal pattern is not very clear, but there is a clear diurnal pattern for c_i/c_a (Fig. 3a). The "*V*"-style c_i/c_a reached its lowest value at around 14:00~15:00 local time. c_i/c_a was higher both in the early morning and late afternoon than noon. As shown in Eq. (3), c_i/c_a depended on both *g* (g_c at canopy scale) and *A* (A_c). High A_c value indicates rapid CO_2 consumption and high g_c values suggesting less resistance for ambient CO_2 entry into intercellular spaces. Therefore, high A_c accompanied by low g_c led to low c_i/c_a. We showed the diurnal pattern of A_c and g_c in Fig. 3b. Both g_c and A_c showed single peak patterns. g_c achieved peak values around 9:00 local time, earlier than that of *A* (peaking around 12:00). These lead to a *V*-style c_i/c_a at diurnal scale (Fig. 3a). The consumption of CO_2 was weak during light-limited periods in the early morning and resulted in the highest c_i/c_a values. Increases in photosynthesis cause a continuous decrease in c_i/c_a, although canopy conductance (g_c) peaked in mid-morning when CO_2 could more readily enter intercellular spaces. c_i/c_a reached its lowest value at around 14:00~15:00 local time; however, this was followed by decreases in A_c and g_c, which led to accumulation of CO_2 in intercellular spaces which increased c_i/c_a.

Response of c_i/c_a to other environmental variables

c_i/c_a was related to several major environmental factors (Fig. 4). Overall, c_i/c_a did not maintain constant values across the entire environmental range. c_i/c_a showed a linear decrease with P_{FD} before light saturation at approximately 0.71 (open triangles in Fig. 4a). The threshold at which P_{FD} shifted c_i/c_a

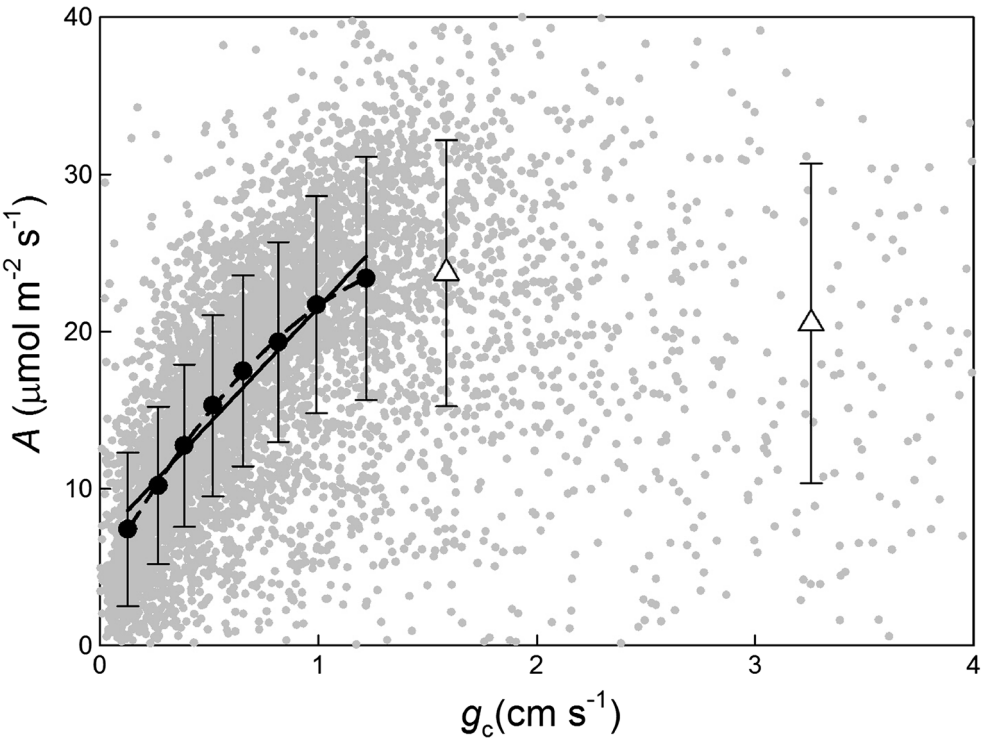

Fig. 1 Relationship between canopy conductance (g_c) and photosynthetic assimilation rate (A_c). *Closed circles* and *open triangles* show the mean of each decile. The *error bars* indicate the standard deviation. The *solid line* represents a linear regression and *dashed line* represents a quadratic regression. Data was collected during January 1 and December 31, 2010

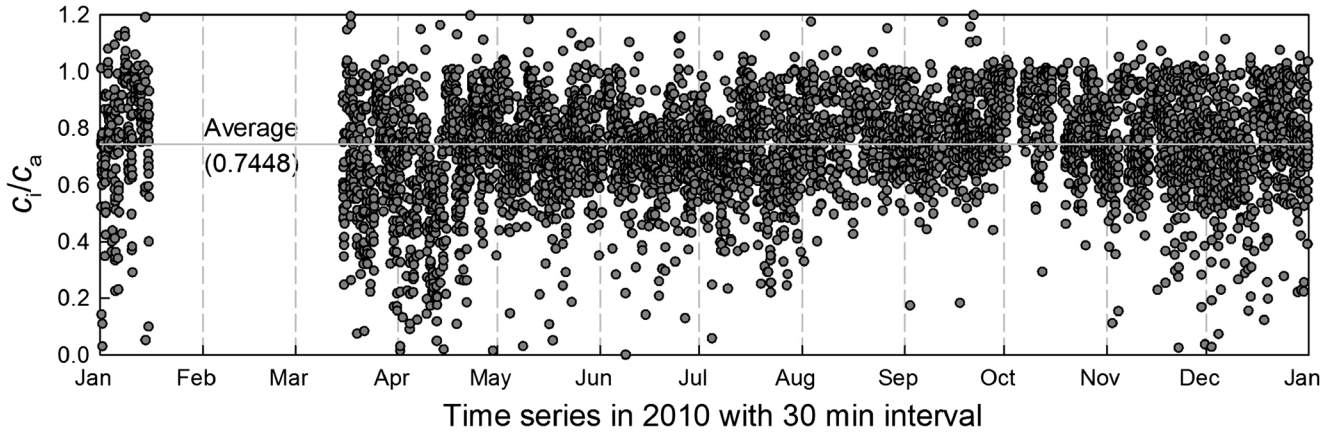

Fig. 2 The time series of intercellular to ambient CO_2 ratio (c_i/c_a). Data was collected during January 1, 2010 and December 31, 2010. The temporal resolution is 30 min. *Gray solid line* indicates the block averaging value of 0.7448. Data during mid-January and mid-March were excluded because of leaf shedding

from light limited to light saturated occurred near 1000 μmol m^{-2} s^{-1}.

Most of the previous studies discussed c_i/c_a under light-saturated conditions. In order to make our results comparable to previous studies, we analyzed environmental response of c_i/c_a with both full-range and light-saturated conditions (Fig. 4). Overall, similar patterns were observed under full-range and light-saturated conditions. c_i/c_a decreases with water vapor deficit (D), increases with soil water content (S_w), and related g_c as described by the model proposed by Katul et al. (2000).

In detail, the linear regression between c_i/c_a and D is expressed as (Fig. 4b, b′)

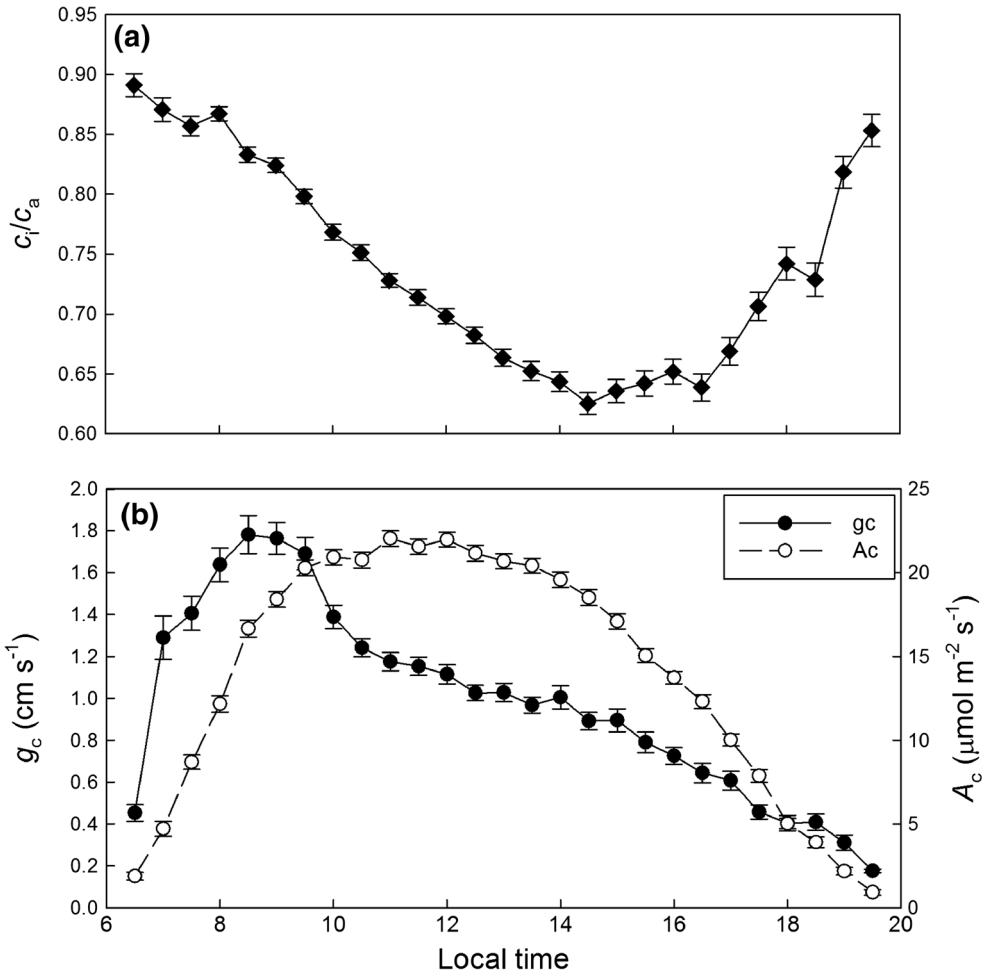

Fig. 3 Mean diurnal variation of c_i/c_a (**a**), canopy conductance (g_c; *close circles* in **b**), and canopy photosynthesis rate (A_c; *open circles* in **b**). All 30-min data in Fig. 2 were used to calculate the mean diurnal pattern here. The *error bars* indicate the standard errors

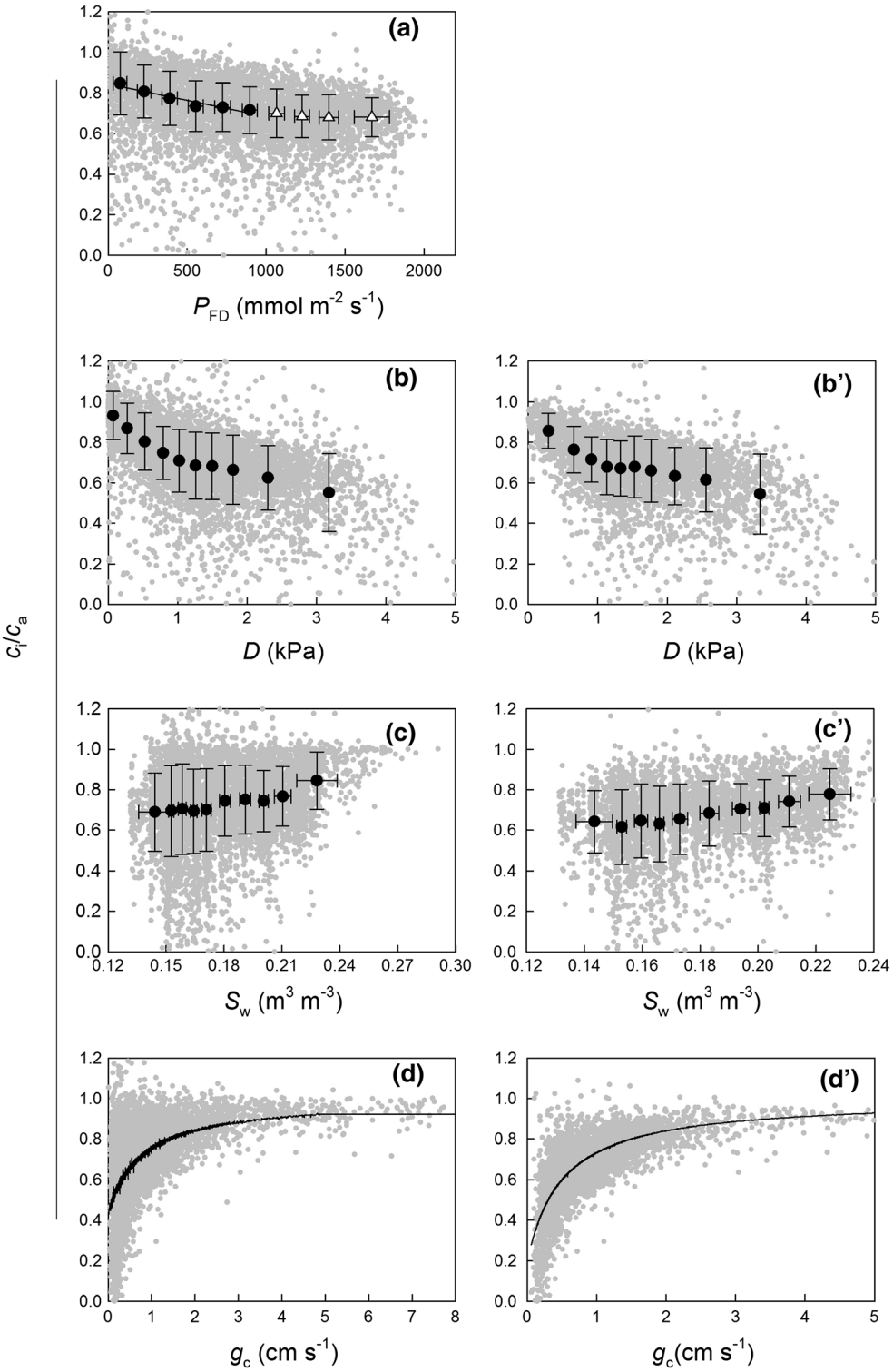

Fig. 4 Dependence of c_i/c_a on environmental factors and canopy conductance. **a**–**d** Data for the full range and (**b′**–**d′**) data only for light-saturated condition. **a** The dependence of c_i/c_a on photosynthetic photon flux density (P_{FD}). **b**, **b′** The dependence of c_i/c_a on water vapor pressure deficit (D). **c**, **c′** The dependence of c_i/c_a on soil water content (S_w). **d**, **d′** The dependence of c_i/c_a on canopy conductance (g_c). *Gray circles* are the 30-min raw data, and *solid black circles* and *open triangles* were the averaging values of each decile. *Error bars* are the standard deviation. The *solid line* in **d** is fitted by Katul 2000 model

$$c_i/c_a = 0.8696-0.1125D\ (r = 0.55, p < 0.001)(\textit{full range}),$$
$$c_i/c_a = 0.8206-0.0892D\ (r = 0.48, p < 0.001)(\textit{light saturated}).$$

c_i/c_a could related to square root of D as

$$c_i/c_a = 0.9808-0.2453\sqrt{D}\ (r = 0.58, p < 0.001)(\textit{full range}),$$
$$c_i/c_a = 0.9447-0.2209\sqrt{D}\ (r = 0.50, p < 0.001)(\textit{light saturated}).$$

Thus, in the statistic perspective, c_i/c_a more probably decreased linearly with the square root of D than with D.

c_i/c_a was shown increased with soil-water status (S_w) (Fig. 4c, c′). Stomatal regulation increases resistance to CO_2 entry under dry conditions; this reduces CO_2 supply causing internal CO_2 depletion and subsequently resulting in low c_i/c_a.

The dependence of c_i/c_a on g_c was well described by the model proposed by Katul et al. (2000) (Fig. 4d, d′). The R_c value (see Eq. (10) for R_c definition) was 0.91. It is near the upper limit value of that from leaf measurements (cf. Fig. 2 from Katul et al. (2000)).

Models describing c_i/c_a behaviors

We compared three models in describing c_i/c_a behavior (see the "Materials and methods" section for detail on these models). Table 1 summarizes the goodness of fit when fitting these models to our dataset. The Jarvis model implemented with four environmental factors (P_{FD}, D, S_w, T_a) work best among all models and expressions (r = 0.6244). The adding of S_w and T could improve model prediction ability. Both Medlyn and Katul models give better statistical fits to our data than other single-variable regressions (Fig. 5 and Table 1). The 1:1 plot suggested that these models have little systematic bias. For all models driven by single D factor, Katul model works best.

Discussion

Whether c_i/c_a is a constant?

In the 1980s, many people believed that stomata could sense c_i and maintain a constant c_i/c_a across wide range of environmental conditions (i.e., Wong et al. 1979; Norman 1982; Baldocchi 1994), and therefore, c_i/c_a supposedly only varied between species, and these constant values were widely used in process-based models. Since species-specific c_i/c_a value could be obtained through isotope recording, a reliable stomatal conductance value could therefore be calculated.

As a case study, our results suggest a necessary of revisit the constant c_i/c_a idea, as there is a substantial and clear diurnal pattern on c_i/c_a (Fig. 3a). Lowest c_i/c_a of around 0.6 occurred in the early afternoon, while highest c_i/c_a of up to 0.9 occurred in the early morning. This *V*-style diurnal pattern c_i/c_a is similar to leaf-level measurements in Czechoslovakia (Marek and Pirochtová 1990), though some differences do exist in both studies. Moreover, c_i/c_a could be related to number of environmental factors (Fig. 4).

Previous studies also challenge the constant c_i/c_a theory. However, most these previous studies have tracked this problem with numeric or modeling approach, especially through stomatal models (i.e., see Katul et al. 2000; Katul et al. 2010; Medlyn et al. 2011). Thus, both our results and those of former studies suggest that c_i/c_a is not a constant but varied across scales and could be related to several environmental driving factors.

How environment factors affect short-term c_i/c_a variations?

As c_i/c_a varies across the day, it is also useful to understand which factors and how they cause the c_i/c_a variations? c_i is determined by A and g_s (see Eq. (3)). As widely known, the major driving factor for A and g_s is P_{FD} and D; it is not surprising that both P_{FD} and D influence c_i/c_a variation (Fig. 4). c_i/c_a decreases with light intensity before P_{FD} reached 1000 μmol m^{-2} s^{-1}. This is consistent with Farquhar and Wong (1984)'s empirical prediction that light limitation enhances c_i/c_a. However, the saturation light intensity is higher than that of leaf experiments (250 μmol m^{-2} s^{-1}; Ball and Critchley 1982) or model simulations (100 μmol m^{-2} s^{-1}; Farquhar and Wong 1984). Multilayer canopies with both sun and shade leaves usually have higher light saturation points for photosynthesis than do individual leaves (cf. Fig.

Table 1 The model performance of three major models in describing c_i/c_a behaviors

Model	Model expressions		Full range		Light saturated	
			r	RMSE	r	RMSE
Jarvis	Expression 1: linear D	c_i/c_a~P_{FD}, D	0.5735	0.1530	0.5174	0.1393
	Expression 2: square root D	c_i/c_a~P_{FD}, $\sqrt{D}$	0.4793	0.1646	0.5358	0.1374
	Expression 3: Lohammer D	c_i/c_a~P_{FD}, D	0.5889	0.1508	0.5279	0.1382
	Expression 4: exponential P_{FD}	c_i/c_a~P_{FD}, D	0.5811	0.1519	0.5258	0.1385
	Expression 5: S_w	c_i/c_a~P_{FD}, D, S_w	0.6123	0.1476	0.5412	0.1369
	Expression 6: S_w, T_a	c_i/c_a~P_{FD}, D, S_w, T_a	0.6244	0.1458	0.5763	0.1331
Medlyn		c_i/c_a~$\sqrt{D}$	0.5837	0.1523	0.5096	0.1405
Katul		c_i/c_a~$\sqrt{D}$	0.5916	0.1506	0.5169	0.1402

The model expressions are shown in the text; see especially Eqs. (17)–(22) for detail of six Jarvis model expressions. The root-mean-squared error (RMSE) and the regression correlation coefficients (r) are shown. Full range showed all data point across light gradient while light saturated showed only data under light saturated conditions

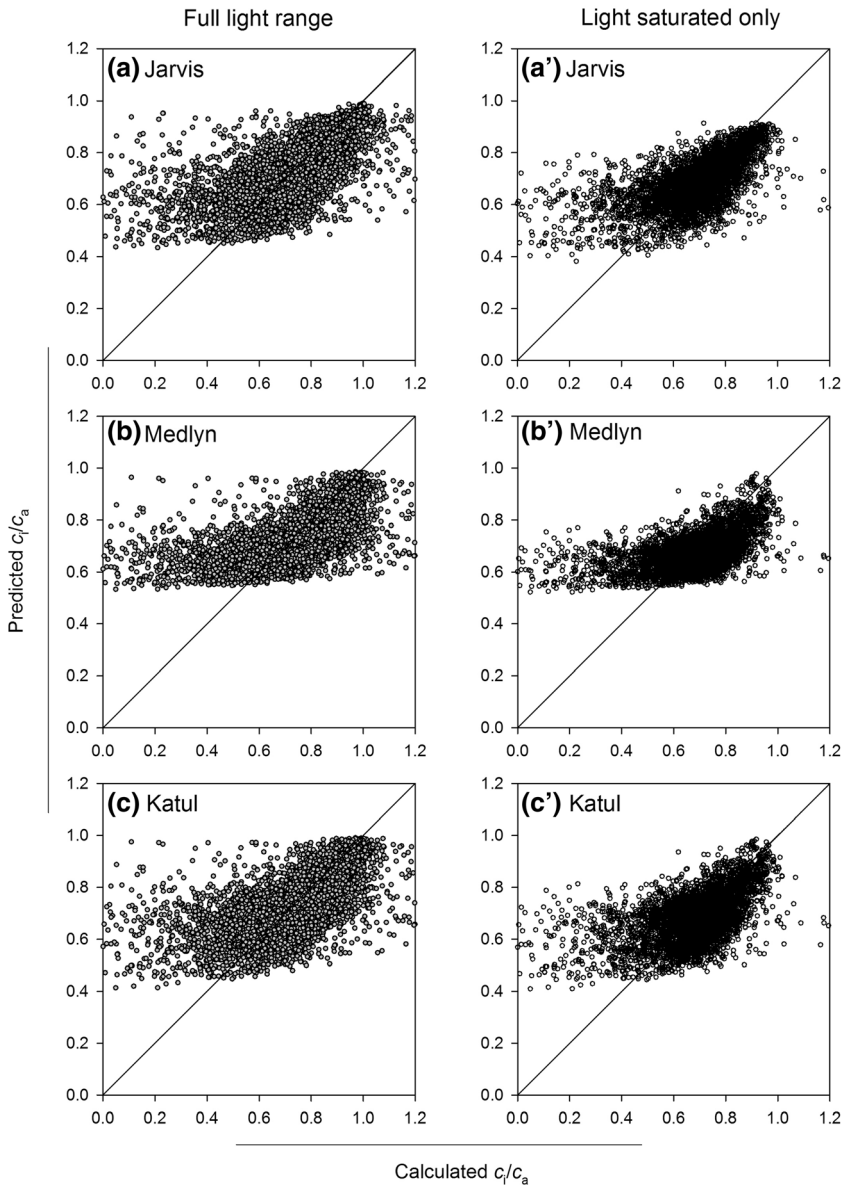

Fig. 5 The 1:1 plot for predicted and calculated c_i/c_a for Jarvis (**a**, **a′**), Medlyn (**b**, **b′**), and Katul 2010 (**c**, **c′**) model. **a**–**c** is for the full light range condition and **a′**–**c′** is for light-saturated condition only. Specifically, the expression (6) of Jarvis model was used for fitting here in **a**. The fitting statistic information could be obtained from Table 1. All model equations could be found within method section of the text

8.8 of Jarvis and Leverenz (1983)), which may explain the high light saturation points for c_i/c_a here.

P_{FD} and D are two intercorrelated factors. When we eliminate the P_{FD} effect by excluding values below light saturation, c_i/c_a was still significantly correlated to D. This suggests that compared to P_{FD}, D plays a much more leading role in controlling c_i/c_a. The subsequent question is in what manner c_i/c_a was controlled by D. The consistent opinion is that c_i/c_a negatively correlated to D (Cowan and Farquhar 1977; Lloyd and Farquhar 1994; Katul et al. 2010; Medlyn et al. 2011). An increasing of D leads to decreasing of c_i/c_a. Stomata tend to close when D increases and thus increases the resistance for CO_2 entering the intercellular space. Intercellular CO_2 becomes scarce if photosynthesis continuously consumes CO_2. However, some studies maintain the view that c_i/c_a decreases linearly with D (Cowan and Farquhar 1977) and the others state that c_i/c_a decreases with square root of D (Lloyd and Farquhar 1994; Katul et al. 2010; Medlyn et al. 2011). We addressed the manner of c_i/c_a decrease with D with our dataset. The correlation coefficient is higher between c_i/c_a and square root of D (0.59) than c_i/c_a and D (0.55) (Fig. 4b, b′). In the statistic perspective, our dataset support that c_i/c_a decreases with square root of D. The single-variable regression (Fig. 4b, b′) has indicated that $\sqrt{D}$ is a better predictor for c_i/c_a. In case of incorporating $\sqrt{D}$ into the Jarvis model, it not works as well as that of D for full light range conditions (Table 1). This apparently conflict findings could be explained as (i) Eq. (18) is in the format of $-(\sqrt{D})$ but not $1/\sqrt{D}$ as that of optimization model and (ii) $-(\sqrt{D})$ was multiplied by the P_{FD} which could exert impact on c_i/c_a predictions.

c_i/c_a also increases with soil water content (S_w) (Fig. 4c, c′). This finding did not directly indicate that S_w has strong

influence on c_i/c_a. This analysis is based on observational but not experimental data. Though we omitted the leaf exchange period data in seasonal analysis, we still could hardly judge this apparent relationship between S_w and c_i/c_a is really caused by the direct effect of S_w or not, because other important seasonal variables vary in the same period. Our explanation for this apparent phenomenon is that stomatal regulation will increase resistance to CO_2 entry under dry conditions; this reduces CO_2 supply causing intercellular CO_2 depletion and subsequently result in low c_i/c_a. Compared to P_{FD} and D (usually subdaily scale), soil water's physiological effect usually takes place on a longer timescale (daily to seasonally). Overall, S_w is a better and observed prediction parameter especially on longer-timescale c_i/c_a studies.

A close relationship was also found between c_i/c_a and g_c (Fig. 4d); this relationship becomes much closer under light-saturated conditions ($r = 0.7636$; Fig. 4d′). This close relationship supports Katul et al. (2000)'s prediction on c_i/c_a and indicates a linearization of A-c_i relationship in our case is effective. The R_c value was 0.90 (full range) and 0.92 (light saturated). It is covered in and near upper limit value of that of leaf measurements (varied from 0.7 to 0.95; cf. Fig. 2 of Katul et al. (2000)). The obtained high c_i/c_a value might be contributed by the following two reasons. First, the gross ecosystem assimilation differed from leaf-level net assimilation was used to calculate c_i (Eq. (6)). This could lead to higher c_i and c_i/c_a values. Second, the tropical tree plantation might matter. Interestingly, Leuning (1995) use a typical tropical tree plantation and obtain R_c value as high as 0.95. Though g_c give better predictions on c_i/c_a than other single environmental variables, such as P_{FD}, D, and S_w, it might be not a good choice to predict the unknown c_i/c_a in the field because g_c is usually not available only when gas exchange measurements were carried out.

As shown above, many factors play roles in driving c_i/c_a variation (Fig. 4), and act in combination. The apparent relationship shown in single-variation regressions may be a consequence of indirect effects by other factors. For example, the P_{FD} and c_i/c_a relationships were not just a light response, but reflect the combined effects of light, temperature, water vapor deficit, and even plant internal factors including leaf water potentials. This calls for deeper analysis. The single-variable regression showed that nonlinear relationships are present. Thus, neither traditional multivariate statistics (i.e., principal component analysis, stepwise regression) nor artificial neuron network could provide competitive description here. We tried a combined model (called Jarvis model) to fill these requirements. The Jarvis model combined g_s, P_{FD}, D, T_a, c_a, and even S_w could be used to describe c_i/c_a variations (Fig. 5a and Table 1). Nevertheless, the model prediction ability did not improve much with the sophisticated structure Jarvis model when compared to single-variable model of D (Fig. 5). Obviously, this finding again stressed the dominant role of D in control c_i/c_a.

How could we model c_i/c_a?

Katul et al. (2000) compared different c_i/c_a models in reproducing photosynthesis. They mentioned, "the physiological complexity in modeling c_i/c_a does not always translate to increased accuracy in predicting photosynthesis." This statement is supported by our dataset; the complex and sophistical Jarvis model did not improve much prediction ability when compared to single D-driving model such as Medlyn and Katul (Fig. 5 and Table 1).

Currently, almost all models for c_i/c_a are based on the stomatal model. Some classic stomatal models have been proposed in the past decades, i.e., Jarvis (Jarvis 1976), Ball-Berry (Ball et al. 1987), Leuning (Leuning 1990; Leuning 1995; Leuning et al. 1995), and recent optimization stomatal model (Katul et al. 2010; Medlyn et al. 2011). Though proposing or establishing a new and better mechanistic model for c_i/c_a is beyond the scope of this study, it is still possible to make a comparison of these already existing models in reproducing our dataset. In this study, the Katul model behaves best in all single D drive models and utilized only one driving variable (D), showing similar prediction ability as that of Jarvis. With same single driving variable, the prediction ability of Katul model is stronger than that of Medlyn. The major difference between Katul and Medlyn models is the stomatal optimization condition: Rubisco-limited (Katul model) and RuBP regeneration-limited conditions (Medlyn model) (Medlyn et al. 2013). Therefore, we favor the idea that stomatal optimization occurs in the Rubisco-limited condition through our dataset.

The Katul model provided a reliable short-time c_i/c_a estimation. The only parameter needed for the model was marginal water use efficiency (λ). Here, we take a fitted λ for our case. In reality, it is practical to obtain λ through leaf gas exchange measurements (Katul et al. 2010). Our λ was estimated to be 0.00158 mol mol^{-1}. In practice, Katul et al. (2010)'s λ could be expressed as

$$\lambda = \left[\frac{c_a}{1.6}\left(\frac{E}{A}\right)^2 \frac{1}{D}\right]^{-1}. \quad (25)$$

The ppm in a gas is normally expressed on a mole fraction basis, so 1 ppm of CO_2 (in the atmosphere) is also 1 μmol per mol. According to Dalton's law of partial pressure, we converted unit of c_a from ppm into partial pressure of Pascal as

$$1\ (\text{ppm}) = 1 \times P_a \times 10^{-6}\ \ (Pascal), \quad (26)$$

where P_a is the atmospheric pressure (Pa). According to dimensional analysis on Eq. (25), λ is dimensionless. To make it consistent when compared to other studies, we set λ in the unit of mol mol^{-1}. This is comparable to that of leaf-level measurement range 0.00033 to 0.00250 mol mol^{-1} and mostly near to

0.00050 mol mol^{-1} (Thomas et al. 1999; please note that the λ of our study is the reciprocal of that in Thomas et al. (1999)'s work due to definition differences). At ecosystem level, λ was reported to be around 0.00200 mol mol^{-1} and varied strongly with CO_2 concentration (Novick et al. 2015; please note that we converted the original unit in μmol mol^{-1} kPa into our unit of mol mol^{-1} with Eq. (26)).

Uncertainties in address c_i/c_a with ecosystem flux measurements

The traditional way to study c_i/c_a uses a leaf chamber under good weather conditions (thus limiting our understanding in other conditions). This was a major motivation for us to address c_i/c_a behavior with ecosystem flux data. The ecosystem fluxes provided by eddy covariance (EC) technique are automatic, continuous, and cover a wide environmental range (Baldocchi et al. 2014). China has established more than 200 eddy flux sites in the past 10 years, covering China's major vegetation types (Xiao et al. 2013), providing the ideal opportunity to address unsolved ecosystem physiology questions.

Nevertheless, EC is not a perfect tool and has some practical constraints and presents some uncertainties. In this study, on c_i/c_a derived from EC fluxes, the constraints and uncertainties are

(i) *EC fluxes present strong random variations*. This is illustrated in Figs. 2 and 5. It is not surprising that EC flux will show negative *NEE* in nighttime, which is physiologically impossible for C_3 plants acting by themselves. This is also why near zero c_i/c_a values occurred in our study.

(ii) *The gross canopy photosynthesis but not net canopy photosynthesis is used in derived c_i*. Strictly speaking, net canopy photosynthesis, the difference between gross canopy photosynthesis and canopy leaf respiration, should be used to derive canopy c_i, which has done in most of leaf-scale studies. However, currently, there is no clear way to separate ecosystem respiration into leaf, branch, stem, root, and soil components. Conversely, most respiration comes from soils (Ryan and Law 2005). Thus, gross canopy photosynthesis is used in this study.

(iii) *Separating transpiration from evapotranspiration*. The EC-based evapotranspiration is the sum of forest floor evaporation, wet canopy evaporation, and transpiration. Forest floor evaporation is usually negligible for closed canopies (Kelliher et al. 1995; Keenan et al. 2013). We adopted a commonly used method to exclude wet canopy data (by excluding rainfall data). This is an empirical method and not and difficult to be validated before this study. It is likely that the values of Fig. 2 at $g_c > 1.5$ cm s^{-1} are affected by canopy wetness.

Though there are some constraints on using eddy flux to address ecosystem c_i/c_a, it facilitates the use of the whole ecosystem as a research unit, automatic monitoring with high temporal resolutions, and nondestructive direct measurements. As a complementary method, using EC technique may enhance our knowledge on c_i/c_a, which cannot come from leaf-level measurements alone. Along with these advanced techniques, uncertainties associated with EC methods should be further reduced to obtain more accurate results.

Conclusions

Investigating c_i/c_a with ecosystem fluxes has seldom been done in the past. Some basic concepts need revision in scaling up from leaf to canopy levels. Here, we used ecosystem fluxes to address c_i/c_a. Overall, we drew several conclusions from this study:

(i) Ecosystem fluxes could successfully be used to address c_i/c_a and develop a more comprehensive understanding of how it functions.

(ii) The c_i/c_a shows a clear diurnal pattern obviously within the environmental gradient. The diurnal pattern of canopy c_i/c_a is *V* shape. c_i/c_a decreases linearly with light intensity under low irradiance but was constant at high irradiances. c_i/c_a decreases with water vapor deficit (*D*) in the manner of square root of *D*. The relationship between c_i/c_a and canopy conductancies was well described by a hybrid model of c_i/c_a and stomatal conductance.

(iii) The water vapor deficit (*D*) is the leading driving factor in cause of the c_i/c_a variation. In general, the Katul stomatal optimization model suggests that optimization occurs during Rubisco-limited conditions, giving the best fitting to our dataset. The inclusion of factors, which vary on longer timescales such as soil water content, may improve the model prediction ability.

Acknowledgements Data of this paper is available by sending e-mail to site principal investigator (wzxrri@163.com). This work was supported by the National Natural Science Foundation of China (31200347, 31660142) and Youth Innovation Promotion Association of Chinese Academy of Sciences.

References

Baldocchi DD (1994) An analytical solution for coupled leaf photosynthesis and stomatal conductance models. Tree Physiol 14:1069–1079

Baldocchi DD (2014) Measuring fluxes of trace gases and energy between ecosystems and the atmosphere: the state and future of the eddy covariance method. Glob Change Biol 20:3600–3609

Ball MC, Critchley C (1982) Photosynthetic response to irradiance by the grey mangrove, *Avicennia marina*, grown under different light regimes. Plant Physiol 70:1101–1106

Ball JT, Woodrow IE, Berry JA (1987) A model predicting stomatal conductance and its contribution to the control of photosynthesis under different environmental conditions. In: Binggins J (ed) progress in photosynthesis research, vol IV.5. M Nijhoff, Dordrecht, pp 221–224

Blanken PD, Black TA, Yang PC, Neumann HH, Nesic Z, Staebler R, den Hartog G, Novak MD, Lee X (1997) Energy balance and canopy conductance of a boreal aspen forest: partitioning overstory and understory components. J Geophys Res Atmos 102:28915–28927

Brodribb T (1996) Dynamics of changing intercellular CO_2 concentration during drought and determination of minimum functional C_i. Plant Physiol 111:179–185

Burba G, Anderson D (2010) A brief practical guide to eddy covariance flux measurements. Principles and workflow examples for scientific and industrial applications. LI-Cor Biosciences, Lincoln

Collatz GJ, Ball JT, Grivet C, Berry JA (1991) Physiological and environmental regulation of stomatal conductance, photosynthesis and transpiration: a model that includes a laminar boundary layer. Agric For Meteorol 54:107–136

Cowan IR, Farquhar GD (1977) Stomatal function in relation to leaf metabolism and environment. In: Jennings DH (ed) Integration of activity in the higher plant. Cambridge Unviersity Press, UK, Cambridge, pp 471–505

Damour G, Simonneau T, Cochard H, Urban L (2010) An overview of models of stomatal conductance at the leaf level. Plant Cell Enivon 33:1419–1438

Farquhar DD, Sharkey TD (1982) Stomatal conductance and photosynthesis. Ann Rev Plant Physiol 33:317–345

Farquhar GD, Wong SC (1984) An empirical model of stomatal conductance. Aus J Plant Physiol 11:191–210

Fick A (1855) Ueber diffusion. Ann Phys 170:59–86

Foken T, Wichura B (1996) Tools for quality assessment of surface-based flux measurements. Agric For Meteorol 78:83–105

Jarvis PG (1976) The interpretation of the variations in leaf water potential and stomatal conductance found in canopies in the field. Phil Trans Royal Soc Lond, Ser B 273:593–610

Jarvis PG, Leverenz JW (1983) Productivity of temperate, deciduous and evergreen forests. In: Lange OL, Nobel PS, Osmond CB, Ziegler H (eds) Physiological plant ecology, IV, ecosystem processes: mineral cycling, productivity and man's influence, 233–280 pp. Springer-Verlag, New York

Katul GG, Ellsworth DS, Lai CT (2000) Modelling assimilation and intercellular CO_2 from measured conductance: a synthesis of approaches. Plant Cell Environ 23:1313–1328

Katul GG, Manzoni S, Palmroth S, Oren R (2010) A stomatal optimization theory to describe the effects of atmospheric CO_2 on leaf photosynthesis and transpiration. Ann Bot 105:431–442

Keenan TF, Hollinger DY, Bohrer G, Dragoni D, Munder JW, Schmid HP, Richardson AD (2013) Increase in forest water-use efficiency as atmospheric carbon dioxide concentrations rise. Nature 499:324–328

Kelliher FM, Leuning R, Raupach MR, Schulze ED (1995) Maximum conductance for evaporation from global vegetation types. Agric For Meteorol 73:1–16

Landsberg J, Sands P (2011) Physiological ecology of forest production: principles, processes and models. Academic Press, San Diego

Leuning R (1990) Modeling stomatal behavior and photosynthesis of *Eucalyptus grandis*. Aus J Plant Physiol 17:159–175

Leuning R (1995) A critical appraisal of a combined stomatal-photosynthesis model for C_3 plants. Plant Cell Environ 18:339–355

Leuning R, Kelliher FM, De Pury DGG, Schulze ED (1995) Leaf nitrogen, photosynthesis, conductance and transpiration: scaling from leaves to canopies. Plant Cell Environ 18:1183–1200

Lloyd J, Farquhar GD (1994) ^{13}C discrimination during CO_2 assimilation by the terrestrial biosphere. Oecologia 99:201–215

Marek M, Pirochtová M (1990) Response of the ratio of intercellular CO_2 concentration to ambient CO_2 concentration (c_i/c_a ratio) to basic microclimatological factors in an oak-hornbean forest. Photosynthetica 24:122–129

Medlyn B, Duursma R, Eamus D, Ellsworth D, Prentice C, Barton C, Crous K, Paolo D, Freeman M, Wingate L (2011) Reconciling the optimal and empirical approaches to modelling stomatal conductance. Glob Change Biol 17:2134–2144

Medlyn B, Duursma R, De Kauwe M, Prentice I (2013) The optimal stomatal response to atmospheric CO_2 concentration: alternative solutions, alternative interpretations. Agric For Meteorol 182–183: 200–203

Mortazavi B, Chanton JP, Prater JL, Oishi AC, Oren R, Katul G (2005) Temporal variability in ^{13}C of respired CO_2 in a pine and a hardwood forest subject of similar climatic conditions. Oecologia 142:57–69

Norman JM (1982) Simulation of microclimate. In: Hatfield JL, Thompson I (eds) Biometeorology and integrated pest management. Academic Press, New York, pp 65–99

Novick KA, Oishi AC, Ward E, Siqueira MBS, Juang JY, Stoy PC (2015) On the difference in the net ecosystem exchange of CO_2 between deciduous and evergreen forests in the southeastern U.S. Glob Chang Biol 21:827–842

Ryan MG, Law BE (2005) Interpreting, measuring, and modeling soil respiration. Biogeochemistry 73:3–27

Tanner CB, Thurtell GW (1969) Anemoclinometer measurement of Reynolds stress and heat transport in the atmospheric surface layer. Department of Soil Science, University of Wisconsin, Madison, WI, Research and Development Technique Report ECOM-66-G22-F to the US Army Electronics Command, 82

Thomas DS, Eamus D, Bell D (1999) Optimization theory of stomatal behavior I. A critical evaluation of five methods of calculation. J Exp Bot 50:385–392

Tissue DT, Barbour MM, Hunt JE, Turnbull MH, Griffin KL, Walcroft AS, Whitehead D (2006) Spatial and temporal scaling of intercellular CO_2 concentration in a temperate rain forest dominated by *Dacrydium cupressinum* in New Zealand. Plant Cell Environ 29:497–510

Vickers D, Mahrt L (1997) Quality control and flux sampling problems for tower and aircraft data. J Atmos Ocea Technol 14:512–526

Webb EK, Pearman G, Leuning R (1980) Correction of flux measurements for density effects due to heat and water vapor transfer. Quart J Royal Meteorol Socie 106:85–100

Wong SC, Cowan IR, Farquhar GD (1979) Stomatal conductance correlates with photosynthetic capacity. Nature 282:424–426

Wu Z (2013) Carbon balance of the rubber plantation ecosystem in Hainan. PhD dissertation, Hainan University, Hainkou, China

Wu Z, Xie G, Yang C, Chen B, Zhou Z (2015) Characteristics of carbon fluxes in a rubber plantation ecosystem in Danzhou area, Hainan Province. J Northwest Forestry Univ 30:51–59

Wu Z, Chen B, Yang C, Tao Z, Xie G, Zhou Z (2012) Distribution of footprint and fluxes source area of rubber plantation in Hainan Island. J Tropical Organ 3:42–50

Wu Z, Chen J, Lan G, Chen B, Xie G, Zhou Z (2013) Quality assessment of turbulence data in rubber plantation ecosystem. Chin J Trop Crops 34:2075–2082

Xiao JF, Sun G, Chen J, Chen H, Chen S, Dong G, Gao S, Guo H, Guo J, Han S, Kato T, Li Y, Lin G, Lu W, Ma M, McNulty S, Shao C, Wang X, Xie X, Zhang X, Zhang Z, Zhao B, Zhou G, Zhou J (2013) Carbon fluxes, evapotranspiration, and water use efficiency of terrestrial ecosystems in China. Agric For Meteorol 182–183:76–90

Zhang H, Nobel PS (1996) Dependency of c_i/c_a and leaf transpiration efficiency on the vapor pressure deficit. Aus J Plant Physiol 23: 561–568